The tribological performance identification of a tire tread block during friction contact: A numerical investigation

Budi Setiyana [1,2*], M. Muchammad [1], Mohammad Tauviqirrahman [1], J. Jamari [1], Eko Saputra [3]

[1] Mechanical Engineering Department, Faculty of Engineering, University of Diponegoro, INDONESIA.
[2] Surface Technology and Tribology Laboratory, Engineering Technology, University of Twente, NETHERLANDS.
[3] Mechanical Engineering Department, State Polytechnic of Semarang, INDONESIA.
*Corresponding author: bsetiyana@yahoo.com

KEYWORDS	ABSTRACT
Tread block SEF Hyper-elastic Yeoh Mooney Rivlin	The tribological performance of tire such as braking capacity (related to contact force) and abrasion resistance (related to surface stress) can be identified through the investigation of the friction contact between tire and road. However, it is difficult to investigate the distribution of contact forces and stress of the tire surface experimentally. As a friction contact model between a tire tread and road surface, a tread block model in contact with a rigid surface is studied here numerically to investigate the distribution of contact forces and stress on its surface. The tread material is a Reinforced Styrene Butadiene Rubber and depicted as a plane strain shape of 15 mm x 10 mm dimension. Analysis was carried out in a constant sliding speed of 300 mm/s with various depths of indentation. Mechanical properties of tread block material was modelled as a hyper-elastic type. The contact forces and stress distribution on the tread block surface were obtained. Results show that dynamic or stick-slip phenomena are observed along friction contact. With respect to the tread block surface coordinate, the surface stress at leading edge is much larger than trailing edge.

1.0   INTRODUCTION

Tribological performance of vehicle tires is often related to abrasion resistance and braking capacity. Abrasion resistance is related to the stress on the tire surface while braking capacity is related to the friction force on the contact between the tire surface and road (Zhang, 2004). Tribological performance is very dependent on the quality of rubber material for tires, especially for tire tread section. There are many types of rubber materials for tires and are currently also undergoing development (Gent, 1992).

Studies on tribology performance on tires have been carried out quite a lot, especially experimentally however, theoretical studies have not been widely presented in some literatures (Podra and Andersson, 1999; Hartung et. Al, 2021; Moldenhauer and Kroger, 2010). In addition to analyse the contact force of the tire surface, experimental studies are generally to observe the phenomenon of abrasion (Fukahori and Yamazaki, 1994; Coveney and Menger, 1999). Meanwhile, theoretical studies are generally to analyse the stress pattern and contact force on the rubber surface (Palfi, et. Al, 2015; Soos and Gooda, 2007). Analysis becomes difficult due to the emergence of vibration or stick-slip phenomena which often appear along friction contact (Setiyana et. Al, 2016; Setiyana et. al, 2018; Khafidh et. Al, 2018, Setiyana et. al, 2021). It can be seen from the fluctuating contact force along sliding contact and periodic wear pattern on the rubber surface due to abrasion (Fukahori and Yamazaki, 1994; Uchiyama and Ishino, 1992).

Theoretical studies are highly dependent on rubber material modelling and analytical methods used. Because of super-elastic and non-linear behaviour of the rubber material, the analysis is generally carried out numerically using Finite Element Analysis (FEA). Due to the narrow of hysteresis band, the rubber material is often modelled as a hyper-elastic material rather than viscoelastic (Gent, 1992; MSC Software Whitepaper, 2010). Regarding the hyper-elastic model, it represents the mechanical properties of rubber material and need constants value of Strain Energy Function (SEF) for input data for simulation using FEA. Strain Energy Function (SEF) states the relationship between stored energy and strain of rubber which in its modelling requires experimental data in the form of tensile test results from rubber specimens (Gent, 1992). There are several experts who propose formulations of SEF such as Mooney-Rivlin, Odgen and Yeoh (Gent, 1992; Liang, 2007).

Tribological performance analysis is related to the contact forces and stress on the tire surface during friction contact however, experimentally, it is very difficult to investigate its distribution along the tire surface, therefore numerical analysis using FEA is required. Related to that, this paper presents a numerical investigation of the tribological phenomena of a tread block model in contact with a flat rigid surface. It is assumed as a friction contact model between a tire tread and road surface. The tread block is subjected to various depth of indentation with a constant sliding speed. The tread block material is a Styrene Butadiene Rubber which is reinforced with carbon black (SBR-25). The analysis is intended to identify the stress and contact forces distribution, especially at the bottom surface of the tread block. This study is expected to obtain an overview of the friction forces that related to braking capacity and the stress that related to distribution of abrasion potential along the tread block surface.

2.0   MATERIALS AND METHOD

This work was carried out numerically using a ABAQUS commercial software package (ABAQUS, 2011). The software requires data about the mechanical properties of rubber expressed by the Strain Energy Function (SEF) constants where the rubber is modeled as a hyper-

elastic material. The SEF constants was obtained from the tensile test data analysis of rubber specimen which in this paper uses SEF from Yeoh version and Mooney-Rivlin version. These versions were chosen because to build these SEF constants can be obtained using uniaxial tensile test data only as was carried out by Liang which applied in this paper (Liang, 2007). The Yeoh version is usually used for filled rubber, while the Mooney-Rivlin version is used for rubber material in general with an assumption that rubber is an incompressible material.

The Strain Energy Function for Yeoh and Mooney-Rivlin version are given at Equation (1) and Equation (2) respectively as following,

$$W = C_{10}(I_1 - 3) + C_{20}(I_1 - 3)^2 + C_{30}(I_1 - 3)^3 \qquad (1)$$

$$W = C_1(I_1 - 3) + C_2(I_2 - 3) \qquad (2)$$

where W is Strain Energy, C_{10}, C_{20}, C_{30}, C_1, C_2 are SEF constants and I_1, I_2 are strain invariant which defined as,

$$I_1 = \lambda_1^2 + \lambda_2^2 + \lambda_3^2 \qquad (3)$$

$$I_2 = \lambda_1^2\lambda_2^2 + \lambda_2^2\lambda_3^2 + \lambda_3^2\lambda_1^2 \qquad (4)$$

$$I_3 = \lambda_1^2\lambda_2^2\lambda_3^2 \qquad (5)$$

The notation λ_1 is extension ratio in main principal coordinate from the tensile test specimen, moreover, λ_2 and λ_3 are extension ratio in others principal coordinate.

Regarding to the Yeoh version, tensile test in filled rubber showed that λ_2 and λ_3 are too small therefore the strain invariant I_1 depends on λ_1 only (Gregory, 1979; Yeoh, 1997). The SEF constants for Yeoh version were obtained by deriving W with respect to I_1 as given in Equation (6) below (Yeoh, 1990),

$$\frac{\partial W}{\partial I_1} = \frac{\sigma}{(\lambda - \lambda^{-2})} = 3C_{30}(I_1 - 3)^2 + 2C_{20}(I_1 - 3) + C_{10} \qquad (6)$$

where σ is engineering stress and λ (= λ_1) is extension ratio from uniaxial tensile test. Meanwhile, by taking $\lambda_1 = \lambda$ and $\lambda_2 = \lambda_3 = \lambda^{-1/2}$ for incompressible material, the SEF constants for Mooney-Rivlin version were obtained using Equation (7) as following (Rivlin, 1956),

$$2\left[\left(\frac{\partial W}{\partial I_1}\right) + \frac{1}{\lambda}\left(\frac{\partial W}{\partial I_2}\right)\right] = \frac{\sigma}{(\lambda - \lambda^{-2})} = C_1 + \frac{C_2}{\lambda} \qquad (7)$$

Rubber material used in this paper is a reinforced Styrene Butadiene Rubber with 25% weight of Carbon Black which is commonly used for tire tread (Liang, 2007). The bulk modulus of the tire rubber material is 0.062 MPa^{-1} with density of 1120 kgm^{-3}. Using the Equation (6) and Equation (7) with tensile test results in the form of the relationship between engineering stress σ and extension ratio λ, the obtained SEF constants for Yeoh version are C_{10}=0.337 MPa, C_{20}=-0.0053 MPa and C_{30}=0.0005 MPa, while the SEF constants for the Mooney-Rivlin version are C_1=0.1218 MPa and C_2=0.4881 MPa (Liang, 2007; Setiyana et. al, 2022).

A schematic illustration of the friction contact on the tread block model and its boundary conditions is depicted in Figure 1. Figure 1(a) depicts the dimensions of the tread block with a

height of 10 mm and a length of 15 mm. Tread block depiction was made in two dimensions in plane strain mode. The top surface of the tread block was pressed with various depths of indentation i. e. 0.6 mm, 0.8 mm and 1.0 mm, while the rigid plate is fixed supported. The tread block model relatively slides on the rigid plate with a constant sliding speed of 300 mm/s. Experimentally, this sliding speed was chosen because this paper is also performed to investigate the dynamic phenomena or stick-slip contact that usually occur in rubber friction, where at a sliding speed of 200 mm/s the friction contact phenomenon is still stationary (Moldenhauer and Kroger, 2010; Setiyana et. Al, 2021). The input data were made as if to represent cases of the braking process. Figure 1(b) shows the FE mesh model of the tread block and rigid flat in an initial condition. The number of elements used in the FE simulation is 6450 elements.
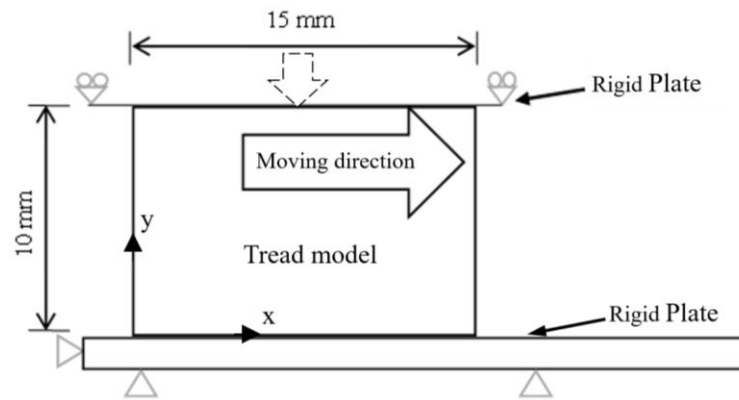
(a)
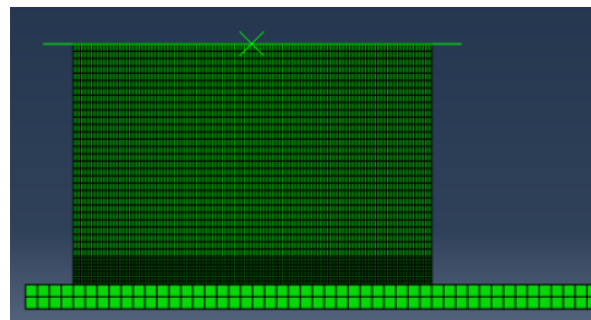
(b)

Figure 1: Simulation modelling of the tread block (a) Schematic model (b) Finite element model.

Analysis was carried out in three conditions, static, stick and slip condition. The static is the condition where the tread block only gets the downward indentation, the stick is the condition when the tread block gets a horizontal action to the right but there is no relative motion between the bottom surface of the tread block and the rigid plate, while the slip is the condition where there is relative motion between the bottom surface of the tread block with the rigid plate. The analysis was carried out with variations in the depth of indentation on the top surface of the tread block and variations of the SEF formulation, namely the Yeoh and Mooney-Rivlin versions. In

conducting the analysis, the observed data are deformation contours, stress pattern and contact forces on the bottom surface of the tread block. The results were presented as a function of time (specifically for the slip condition) and as a function of the horizontal distance x at the bottom surface of the tread block.

3.0   RESULTS AND DISCUSSION

3.1   Deformation Contour and Stress Pattern

The deformation contour and stress pattern with the depth of indentation of 1.0 mm on the tread block are given in Figure 2 for the static condition, Figure 3 for the stick condition and Figure 4 for the slip condition. The numerical simulation results are given for both SEF versions. The stress is displayed in von Mises mode and assigned value for the static phase only. It can be seen that the deformation and stress have similar patterns between the two SEF versions, especially for static and stick conditions. For the slip conditions the degree of similarity of both SEF modes is qualitatively reduced. The stress pattern for the slip condition is taken at the same time.
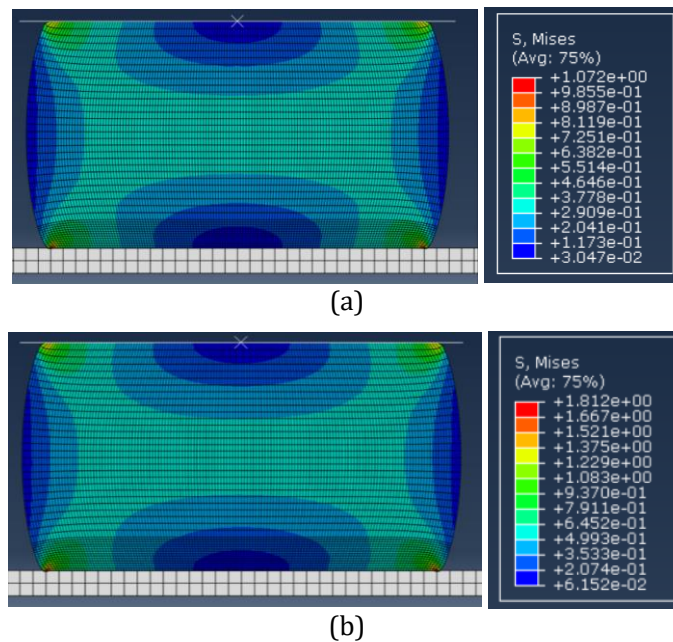

(a)

(b)

Figure 2: Contour of stress and deformation at static condition for both SEF versions (a) SEF of Yeoh (b) SEF of Mooney Rivlin.
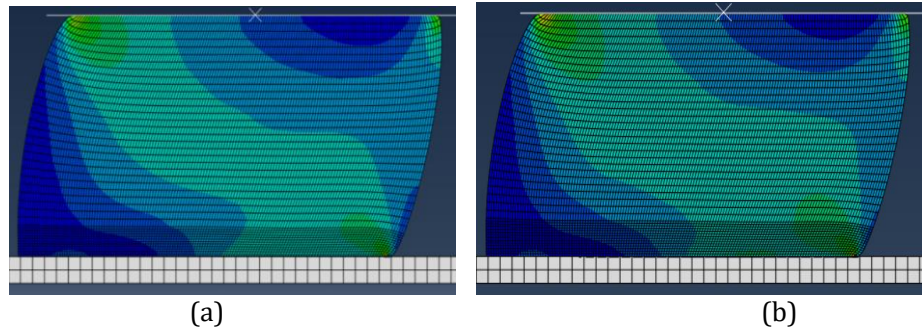
Figure 3: Contour of stress and deformation at stick condition for both SEF versions (a) SEF of Yeoh (b) SEF of Mooney Rivlin.
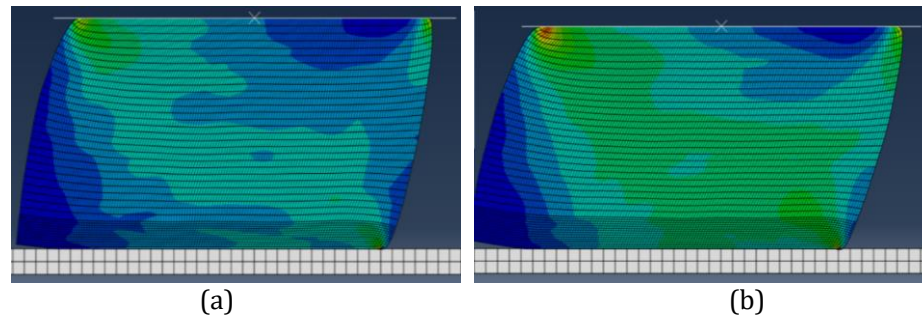

Figure 4: Contour of stress and deformation at slip condition for both SEF versions (a) SEF of Yeoh (b) SEF of Mooney Rivlin.

From the Figures can be seen that the stress of the Mooney-Rivlin version is larger than that of the Yeoh version. This expreses that the Mooney-Rivlin version has a higher material stiffness assumption than the Yeoh version. Under the static conditions, SEF Yeoh produces a maximum stress of 1,072 MPa and for Mooney-Rivlin it produces 1,812 MPa. The stress value for the stick and slip conditions are not shown here. As for the maximum stress value in the stick condition, for SEF Yeoh it is 1,546 MPa and for Rivlin it is 2,545 MPa. While the maximum stress in the slip condition, SEF Yeoh produces a value of 1.53 MPa and for Rivlin produces a value of 2.372 MPa.

3.2   Stress and Contact Forces Fluctuation
The numerical simulation results in the time function are given at the initial conditions of the slip phase during the first 0.1 seconds. The presented results are the maximum stress that occurs in a particular element and the contact forces on the bottom surface of the tread block. Figure 5 shows the stress with varying depth of indentation for the two versions of SEF. It can be seen that there are fluctuations during the slip phase and the Mooney-Rivlin version gives a larger stress than the Yeoh. The fluctuations are especially noticeable for large depth of indentation.
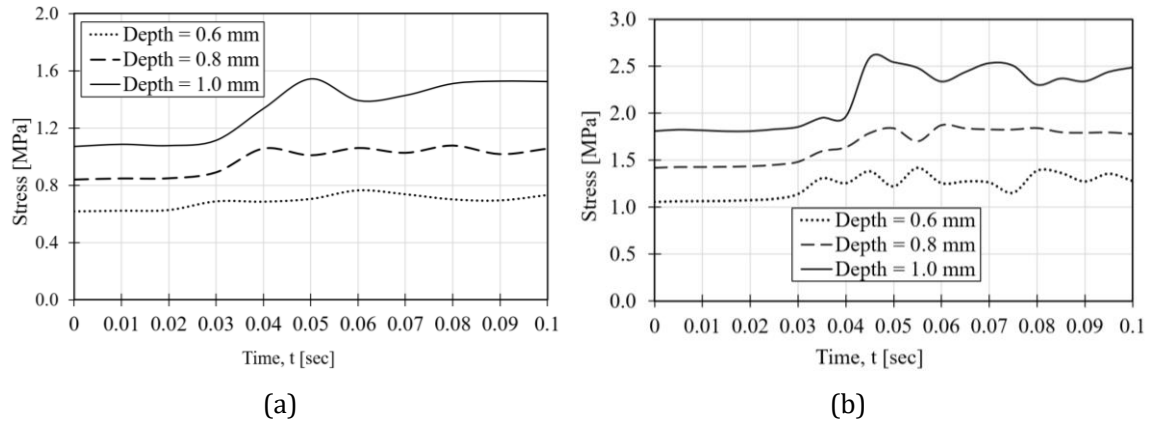
(a) (b)

Figure 5: The fluctuating stress of the certain element at the beginning of the slip phase (a) SEF of Yeoh (b) SEF of Mooney Rivlin.
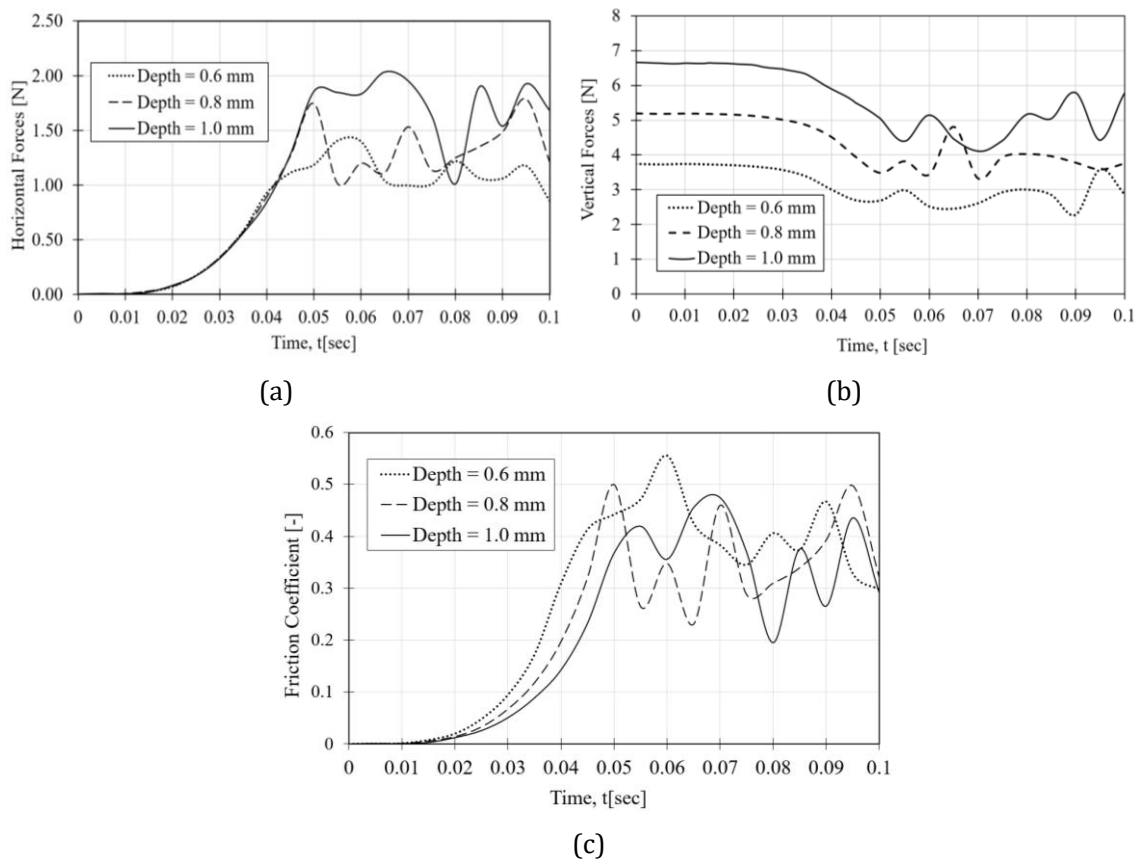

(a) (b)

(c)

Figure 6: The fluctuating contact forces at the bottom surface for SEF of Yeoh at the beginning of slip phase (a) Horizontal forces (b) Vertical forces and (c) Friction Coefficient.

Figure 6(a) dan Figure 6(b) show the fluctuation of the contact force at the beginning of the slip phase at the bottom surface of the tread block, namely the horizontal force (friction force) and the vertical force for Yeoh's SEF version. As it starts to slip, the horizontal force increases drastically until it starts to fluctuate around 0.05 second. For the vertical or normal force, the contact force decreases slightly and then begins to fluctuate at 0.05 seconds. In general, it is seen that the larger depth of indentation, the larger the contact force. The phenomenon of fluctuations in the contact force is indeed often encountered in friction on rubber materials and is often referred to as the stick-slip phenomenon. Figure 6(c) shows the coefficient of friction which is the ratio between the horizontal force and the vertical force. From the figure it can be seen that the value of the friction coefficient begins to fluctuate starting at 0.05 seconds and have average values that are almost the same for variations in the depth of indentation, which is around 0.5. This graph is constructed still with the assumption that the contact surface is really smooth so that the friction coefficient due to surface roughness is omitted. It has been noted that the horizontal force consists of adhesion component due to surface roughness and deformation component due to elastic resistance (Gent, 1992).

3.3   Stress and Contact Forces Distribution

The stress distribution of the elements at the bottom surface of the tread block is given in Figure 7 at a certain moment in the slip phase. The stress distribution is given for both SEF versions with respect to the horizontal distance of the bottom surface (x-axis). It can be seen that the stress at leading edge much larger than trailing edge and the Mooney-Rivlin version is higher than the Yeoh. The trend of the stress distribution of the two versions is similar, at the left end the value is zero and at the right end the value is largest. The larger depth of indentation the larger stress. The stress distribution on the surface elements is of course related to the distribution of abrasion potentials, that the larger the stress provides the larger the abrasion potential.

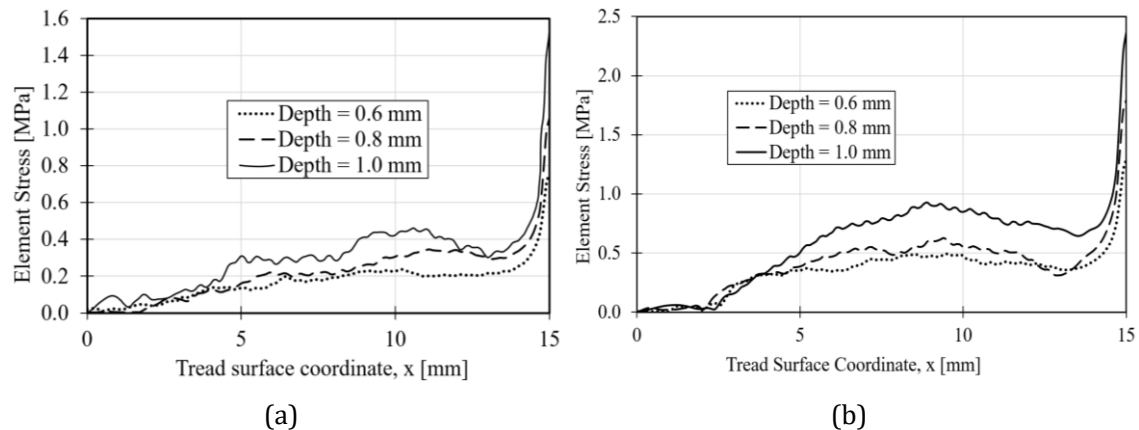(a)   (b)

Figure 7: Stress the elements at the bottom surface in the beginning of slip phase (a) SEF of Yeoh (b) SEF of Mooney Rivlin.

The distribution of the contact force for each node at the bottom surface of the tread block is given in Figure 8, Figure 9 and Figure 10 for the static, stick and initial slip condition respectively. The contact forces shown are the horizontal force and the vertical force for Yeoh's version of SEF with varying depths of indentation. For the static contact as shown in Figure 8, it can be seen that

the resulting contact forces give a symmetrical value. For the horizontal force, the left tread section receives the right-directed contact force and the right tread section receives the left-directed contact force. The vertical or normal contact force shows symmetrical data with maximum values at both ends.

Figure 9 shows the contact force when entering the stick phase where the contact forces value is no longer symmetrical. For the horizontal force, the majority of the force acts to the left as a form of resistance to the force acting to the right given to the tread block. At a value of about 6.0 mm, there is a transition of the friction force from the right direction to the left direction. The vertical force is also no longer symmetrical and the right side of the tread block receives a larger normal force than the left side as a form of resistance to the action force applied on the tread block.
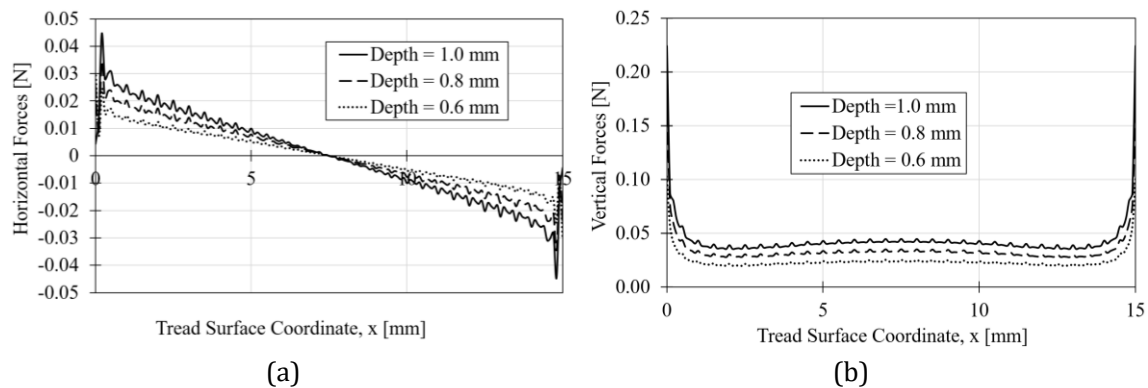

Figure 8: Contact forces at the bottom surface in static condition for SEF of Yeoh (a) Horizontal forces (b) Vertical forces
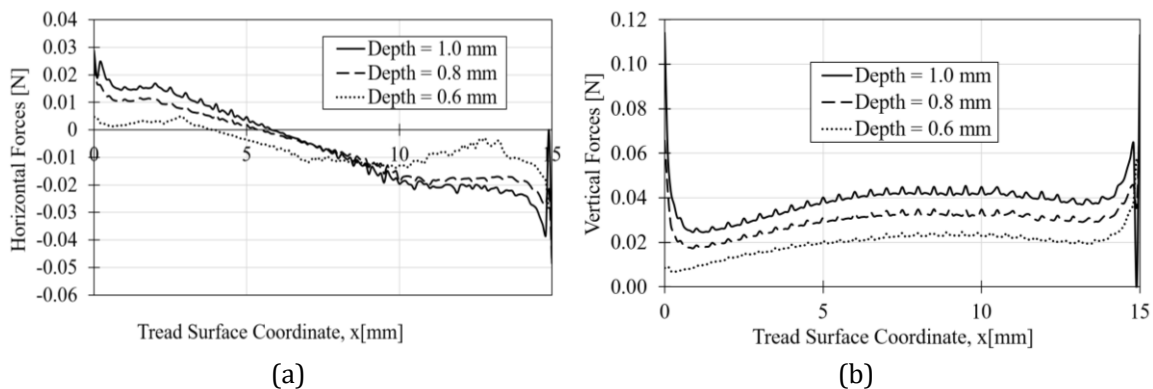

Figure 9: Contact forces at the bottom surface in stick condition for SEF of Yeoh (a) Horizontal forces (b) Vertical forces.
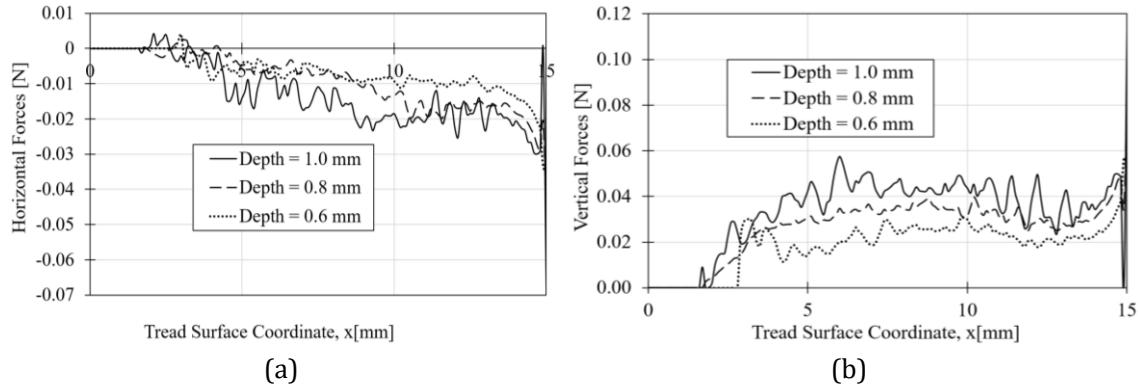
Figure 10: Contact forces at the bottom surface in the beginning of slip phase for SEF of Yeoh (a) Horizontal forces (b) Vertical forces.

The surface contact force at the start of the slip phase is given in Figure 10, where the majority of the horizontal contact force has a negative value. This indicates resistance to the action force on the tread block. While the vertical contact force indicates that the left end of the tread has practically no contact force and the dominant vertical force is in the middle and right section. Both horizontal and vertical forces show fluctuating values with respect to the distance (x-axis) which indicates fluctuations of the bottom surface of the tread block to its counter surface.

There are several notes regarding the simulation results above. The contact forces and stress data with respect to time are fluctuating which show the emergence of dynamic phenomena that is often called as stick-slip phenomena, that commonly occur in rubber friction (Setiyana et. Al, 2016; Setiyana et. Al, 2021). The distribution of contact forces under static conditions along tread block surface provides symmetrical results between the leading edge and trailing edge, which logically must be like that. Meanwhile, in the stick condition, the contact force distribution tends to be larger on the leading edge compared to the trailing edge and then this condition is very clearly visible in the slip condition. This will of course provide a large compressive stress on the leading edge. Regarding the contour of stress distribution along the tread block surface, the stress at leading edge is much higher while the trailing edge is very small, where it is qualitatively similar to the contour of an abraded tread block surface performed by Moldenhauer (Moldenhauer and Kroger, 2010).

CONCLUSIONS

This work is developed to numerically investigate the phenomena in friction contact between a tread block model and a rigid flat surface. This is carried out to identify the tribology performance, especially related to the distribution of stress and contact force along the tread block bottom surface. The analysis was carried out by varying the depth of indentation on the top tread surface with a constant sliding speed. Based on the simulation and analysis results, it can be seen that Mooney-Rivlin version of the SEF provides larger stress than the Yeoh, even though it has a similar stress pattern. This applies to all conditions, static, stick and slip conditions.

During the slip phase, the stress, contact force and friction coefficient fluctuate with time, which is known as the stick-slip phenomenon. The stress distribution along the bottom surface of the tread block gives a similar distribution for both SEF versions. The maximum stress occurs at

the leading edge of the tread facing the direction of motion and much higher than the trailing edge. The distribution of the contact force on the bottom surface of the tread is given under all conditions, namely the static, stick and slip condition. In the static phase, the distribution of the contact force is symmetrical and the distribution changes as it enters the stick phase. At the beginning of the slip phase, the majority of horizontal or frictional forces oppose the action force exerted on the tread block to move. In slip conditions, the contact force on the trailing is very small, even as if there is no contact between the tread block and the rigid flat surface.

The stress distribution at the bottom surface of the tread is closely related to the distribution of the potential for abrasion, where the high potential for abrasion occurs at the leading edge of the tread block. Meanwhile, the braking capacity during pure sliding is closely related to the friction force, the larger depth of indentation provides the larger friction force. In this paper, the value of friction coefficient during the slip phase has relatively the same value for various depth of indentation even though there are fluctuations.

ACKNOWLEDGMENT

REFERENCES

ABAQUS 6.11. (2011). Standard User's Manual, Dassault Systems Simulia Corp., USA.

Coveney, C. & Menger, C. (1999). Initiation and development of wear of an elastomeric surface by a blade abrader. Wear 233-235, 702-711.

Fukahori, Y. & Yamazaki, H. (1994). Mechanism of rubber abrasion—Part 2: General rule in abrasion pattern formation in rubber-like materials. Wear, 178, 109-116.

Fukahori, Y. & Yamazaki, H. (1994). Mechanism of rubber abrasion—Part 1: abrasion pattern formation in natural rubber vulcanizate. Wear, 171, 195-202.

Gent, A.N. (1992). Engineering with Rubber, How to design rubber components, 3rd edition, Hanser Publication, Cincinnati, USA.

Gregory, M. J. (1979). The stress-strain behaviour of filled rubbers at moderate strains. Plastics and Rubber: Material and Application 4, 184-188.

Hartung, F., Garcia, M. A., Berger, T., Michael Hindemith, M., Wangenheim, M. & Kaliske, M. (2021). Experimental and Numerical Investigation of Tire Tread Wear on Block Level. Lubricants 2021, 9, 113.

Khafidh, M., Setiyana, B., Jamari, J., Masen., M.A. & Schipper, D.J. (2018). Understanding the occurrence of wavy track of elastomeric material. Wear, 412-413, 23-29.

Liang, H. (2007). Investigating the mechanism of elastomer abrasion, Doctoral Thesis, University of London, London.

Moldenhauer, P. & Kroger, M. (2010). Simulation and Experimental Investigations of the Dynamic Interaction between Tire Tread Block and Road. Elastomere Friction, LNACM 51, pp. 165–200.

MSC Software Whitepaper. (2010). Nonlinear Finite Element Analysis of Elastomer, MSC Software Corporation, Santa Ana, USA.

Palfi, L., Goda, T., Varadi, K., Garbayo, E., Bielsa, J.M. & Jiménez, M.A. (2015). FE prediction of hysteretic component of rubber friction. Advances in Tribology, 2012, 2-13.

Podra, P. & Andersson, S. (1999). Simulating sliding wear with finite element method. Tribology International 32, 71-81.

Rivlin, R. S. (1956). Large elastic deformations. Rheology 1, Academic Press, New York, 351.

Setiyana, B., Ismail, R., Jamari, J. & Schipper, D.J. (2016). Stick-slip behaviour of a viscoelastic flat sliding against a rigid indenter. Tribology Online, 11,3, 512-518.

Setiyana, B., Ismail, R., Jamari, J. & Schipper, D.J. (2018). Analytical study of the wear pattern of an abraded rubber surface: Interaction model. Tribology, Material Surface and Interfaces, 12(4), 186-192.

Setiyana, B., Jamari, J., Ismail, R. & Schipper, D.J. (2022) A numerical investigation of the sliding contact between a rigid spherical indenter and a rubber surface: The effect of sliding depth and surface roughness. Jurnal Tribologi 33, 20-30.

Setiyana, B., Khafidh, M., Tauviqirrahman, M., Ismail, R., Jamari, J. & Schipper, D.J. (2021). Friction and Wear Pattern of Silica-Reinforced Styrene-Butadiene Rubber (SBR) in Sliding Contact with a Blade Indenter. Lubricants 9, 110, 1-13.

Soos, E. & Gooda, T. (2007). Numerical analysis of sliding friction rubber behaviour. Trans Tech Publication, 537-538, 615-622.

Uchiyama, Y. & Ishino, Y. (1992). Pattern abrasion mechanism of rubber. Wear, 158, 141-155.

Yeoh, O. H. (1997). Characterisation of Elastic Properties of Carbon Black Filled Rubber Vulcanizates. Rubber Chemistry and technology 63, 792-805.

Zhang, S.W. (2004). Tribology of Elastomer, Tribology and Interface Engineering Series, 1st Edition, Elsevier, Amsterdam.